Results from Auger

R. C. Shellard for the Auger Collaboration
CBPF, Rio de Janeiro, RJ 22280-180, Brazil

The Pierre Auger Observatory, being constructed in the Mendoza Province, Argentina is optimized to study the main characteristics of the ultra high energy cosmic rays at energies greater than 10^{19} eV. The observatory addresses this challenge by collecting a large statistical sample of air-showers, using two complementary techniques, a large array of ground based particle detectors, overlooked by a set of telescopes trained at the fluorescence light emitted as the showers transverses the atmosphere.

1. INTRODUCTION

The cosmic ray spectrum, measured at the top of the atmosphere covers a huge range in energy, going from 10 MeV to energies above 10^{20} eV, with a differential flux that spans 31 decades (Nagano and Watson [2000]). The techniques to survey this spectrum goes from instruments aboard satellite flights, balloon borne detectors, to counters that monitor the fluxes of neutrons and muons at the Earth surface, and at higher energies to wide area arrays of particle detectors. The spectrum can be divided roughly into four regions with very distinct behavior. The first one, with energies below 1 GeV, has a very distinctive character from the rest of it. Its shape and cut-off is strongly dependent on the phase of the solar cycle, a phenomenon known as *solar modulation*. Actually, there is an inverse correlation between the intensity of cosmic rays at the top of the atmosphere and the level of the solar activity (Longair [1992], Shea and Smart [1985]).

Figure 1: The Pierre Auger Observatory building in the City of Malargüe, in Argentina. The large room on the second floor, with the big window houses the Central Data Acquisition system of the experiment. The large room on the ground floor is the Visitor's Center of Auger.

The region above 1 GeV show a spectrum with a power law dependence, $N(E)\ \mathrm{d}E = K\ E^{-x}\ \mathrm{d}E$, where the spectral index x varies as $2.7\ <\ x\ <\ 3.2$. The region between 1 GeV and the *knee* region at 4×10^{15} eV, is characterized by an index $x\ \simeq\ 2.7$. These cosmic rays most likely are produced at supernova explosions and their remnants (Aharonian et al [2004]). At the knee (4×10^{15} eV) the power law index steepens to 3.2 until

the so called *ankle*, at 5×10^{18} eV. The origin of the cosmic rays in this region is less clear and subject of much conjecture. Above the ankle the spectrum flattens again to an index $x \simeq 2.8$ and this is interpreted by many authors as a cross over from the steeper galactic component to a harder extra galactic source for the cosmic rays (Cronin [1999], Olinto [2000]).

The existence of cosmic rays with energies above 10^{20} eV presents a puzzling problem in high energy astrophysics. The first event of this class of phenomena was observed at the beginning of the 60's by John Linsley at the Volcano Ranch experiment, in New Mexico (Linsley [1963a,b]). Since then, many events were detected, at different sites, using quite distinct techniques (Bird et al. [1993], Efimov et al. [1991], Lawrence et al. [1991], Takeda et al. [1998], S.Yoshida et al. [1997]). If those cosmic rays are common matter, that is, protons, nuclei or even photons, they undergo well known nuclear and electromagnetic processes, during their propagation through space. Their energies are degraded by the interaction with the cosmic radiation background (CMB), way before they reached the Earth (Greisen [1966], Zatsepin and Kuzmin [1966]). After travelling distances at the scale of 50 Mpc, their energies should be under 10^{20} eV, thus restricting the possible conventional astrophysical objects, which could be sources of them, and those should be easily localized through astronomical instruments. On the other hand, it is very difficult to explain the acceleration of charged particles, with energies up to 3×10^{20} eV or even greater, on known astrophysical objects, by means of electromagnetic forces, the only conventional ones capable of long range and long periods of acceleration.

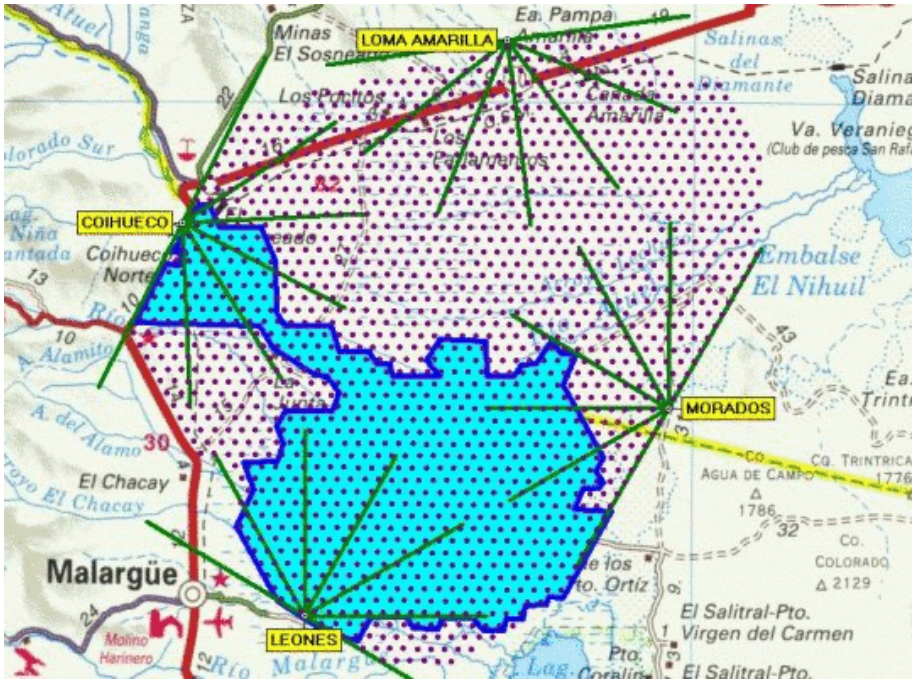

Figure 2: Layout of the Pierre Auger Observatory southern site showing the four FD telescopes (*eyes*). The dots represnts the deployement location of the SD stations. The darker shade represents the area instrumented in November 2004.

2. COSMIC RAY DETECTORS

The ultra high energy cosmic rays hit the air molecules starting an extensive air shower as the fragments of the first collision hit other nuclei, producing cascades of pions. The neutral pions start an electromagnetic shower of photons, electrons and positrons. The charged ones will strike other atoms or decay into muons and

Figure 3: The Assembly Building with the water tower at the back. Behind the front-right tank there is a flatbed truck unloading its cargo of six tanks.

neutrinos or eventually survive until the ground. The extensive air shower can be imagined as a very thin pancake of particles, gammas, electrons, positrons, muons and some hadronic matter, crossing the atmosphere at the speed of light. The atmosphere works as a giant calorimeter, were the Molière radius is of the order of 76 m, in contrast to the few cm which it is in lead. The core of the disk has a high density of particles which then falls sharply as one get away from it. For cosmic rays at 10^{20} eV, the lateral density of particles can still be above one charged particle per square meter at distances of a few kilometers from the core of the shower. A very rough estimate of particle content of a shower is that for every muon, there are about 10 electrons or positrons and 100 photons. This rule of thumb depends very much on the zenith angle and the stage of the shower development. Measuring this ratio would lead to clues about the primary chemical composition of the cosmic ray.

To measure the cosmic rays one may take a snapshot of the cross section of the shower, as it hits the ground. However, as the flux is very low, one has to expose an extensive area, which runs into thousands of square kilometers in the experiments which are being built today. A typical arrangement consists of measuring stations, with an exposure area of a few square meters, which is sensitive to the amount of particles that transverses it. The stations are spread over a large areas, with a separation between them dependent on the threshold of energy one wants to set in the array. The footprint of a typical 10^{19} eV shower is about 10 km^2, so that a separation of 1.5 km between the stations will activate about 10 stations, allowing for a good direction reconstruction. The separation between stations vary among the surface arrays, but are typically on the range between a few hundred meters and a little above 1.5 km. The angular resolution in this sort of array is better than 3°. The detector stations in this class of arrays are either scintillation counters or Čerenkov detectors. Some arrangements use buried scintillation counters to identify the muonic component of a shower. The energy of the shower is identified by the density of charged particles in a ring, at a large distance from the core, typically about 600 m (Hillas [1970]). The correlation between this density and the primary energy is inferred from shower simulation and is quite independent of the primary composition. The identification of the primary chemical composition using surface arrays is difficult, for it relies on subtle differences on the muonic radial distribution in relation to the electromagnetic component of the shower (Walker and Watson [1981, 1982]), as well as the detailed structure of the shower front.

Figure 4: Tank being loaded to a 4-wheel vehicle for final deployment.

The other technique which has been used to measure the ultra high energy cosmic rays, make use of the light emitted by the fluorescence of the excited nitrogen atoms and molecules along the path of the shower. This light, emitted mostly in the UV region, with wavelength between 300 and 400 nm, can be collected by telescopes standing far away. The yield of photons varies very little with the altitude, about 4 photons per meter of electron track of the shower (Nagano et al. [2004]). The intensity of their emission is proportional to the total number of electrons tracks at each stage of the shower, giving a longitudinal profile measurement of the shower development. This allows for a direct and more precise measurement of the energy of the shower, without dependence on theoretical models for showers. The direction of the shower is extracted from a geometrical reconstruction of the evolution of the signal.

The depth of the shower maximum (defined in g/cm^2) for a given energy is dependent on the primary composition of the cosmic ray. The measurement of X_{max}, the position of maximum development of the shower, with sufficiently fine resolution, will be a discriminator on the nature of the primary cosmic ray particle. However, fluorescence detectors have a drawback, for they can be operated only at night, when the sky is clear and moonless, which in practice amounts to a 10% duty cycle during the year.

3. THE PIERRE AUGER OBSERVATORY

The Pierre Auger Observatory (Auger Collaboration [1996, 2001]) is designed to study the higher – above 10^{18} eV – end of the cosmic ray spectrum, with high statistics over the whole sky. The detectors are optimized to measure the energy spectrum, the directions of arrival and the chemical composition of the cosmic rays, using two complementary techniques, surface detectors based on Čerenkov radiators and fluorescence light detectors. The complete project calls for two sites, one in the southern hemisphere, already in construction, and a northern site, in order to achive the homogeneous coverage of the whole sky, essential to pinpoint the sources of the ultra high-energy cosmic rays.

The southern site of the Observatory, located in the province of Mendoza, in Argentina, at the latitude 35° South and longitude 69° West, on a very flat plateau at 1 400 m above sea level, is bounded by the Andes on the west. The region has a very clear sky, with little light pollution, essential for the operation of the fluorescence system. The main office of the observatory, shown in Figure 1, is located at the northern entrance of the City

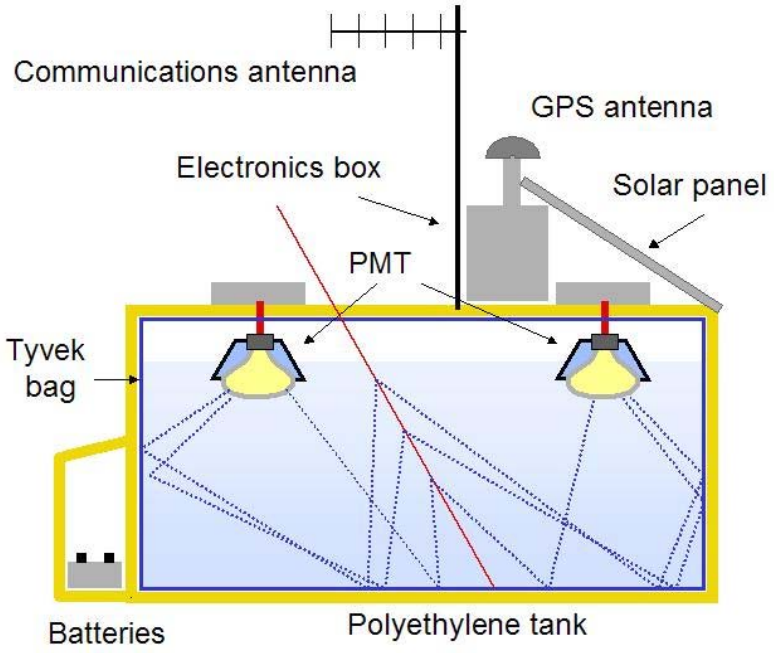

Figure 5: A schematic view of the Čerenkov water tanks, with the components indicated in the figure.

of Malargüe. The construction of the northern site, in the United States, will start in 2006.

The Surface Detector (SD) is a ground array which spans an area of 3 000 km^2, with 1 600 stations set on a regular triangular grid, with 1 500 m separation between them. The stations communicate with the central base station through a radio link. The whole array is overlooked by four Fluorescence Detectors (FD), laid in its periphery. A map of the area indicating the location of the tanks and of the fluorescence telescopes is shown in Figure 2.

The initial phase of the Pierre Auger Observatory, the *Engineering Array* was built during the period 2000-2001. Then, 40 Čerenkov tanks were laid and instrumented, to test the components of the array and to prove the soundness of its design. They were set in a roughly hexagonal array, covering an area of 54 km^2. Two of the tanks, at the center of the array, were laid side by side, in order to cross calibrate their signals. Two prototype telescopes were installed on the Los Leones hill, overlooking this ground array. They were successfully tested during the southern summer of 2001-2002. The lessons learned in the Engineering Array lead to improvement in the final design of the detector components (Abraham et al [2004]).

3.1. THE SURFACE DETECTOR

Each station at the SD is a cylindrical tank, filled with 12 000 l of purified water, operating as a Čerenkov light detector. The tanks are manufactured by rotational molding process, using a high density polyethylene resin, with 12.7 mm thick walls, opaque to external light. The walls have two layers, an external in the color beige, to minimize the environmental impact and reduce the heat absorption, and the internal black, with the addition of carbon black to the resin. The water is contained in a liner inside the tank, a bag made of a sandwich of polyolefin-Tyvek film. The Tyvek film has a high reflectivity to ultraviolet light and its role is to diffuse the UV Čerenkov light within the volume of water.

The tanks are prepared in the Assembly Building, just behid the Main campus building. The water purification plant produces enough water for 3 tanks per day, with a resistivity of 15 MΩ per cm. The building and the water

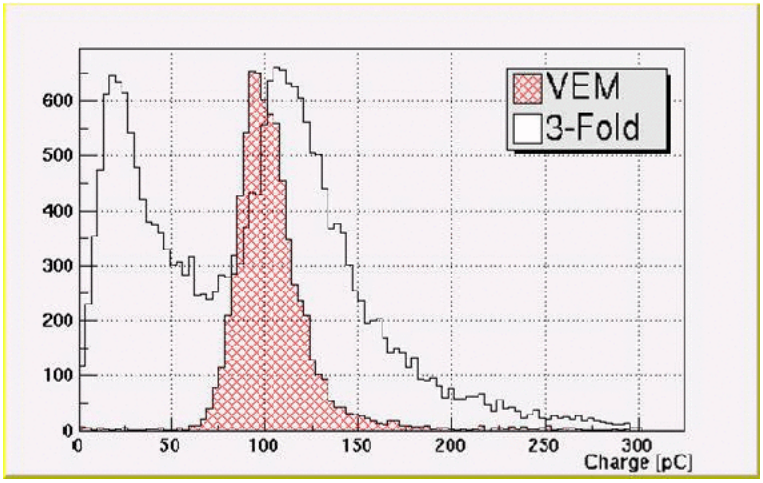

Figure 6: Typical histogram used in the calibration of the surface stations. This was taken from a prototype tank equipped with scintillation pads to select the component of the signal due to vertical muons. The hump of the experimental distribution of single muons is related to the signal due to a vertical incoming muon (Bonifazi [2004]).

tower is shown in Figure 3. The tanks are manufactured in São Paulo, Brazil, and Buenos Aires and shipped all the way to Malargüe on flatbed trucks, carrying six tanks on a load. After preparation which includes the mounting of the electronic components, the cabling and fitting the internal Tyvek bag, the tanks are deployed on the field, on prepared ground, using 4-wheel drive vehicles (Figure 4).

The Čerenkov light, diffused within the volume of water, is collected by three 20.3 cm diameter photomultiplier tubes (Photonis XP1805), set in a symmetric pattern on top of the tanks, facing downwards. This arrangement avoids the direct hit of the Čerenkov light, collecting a signal which is homogeneous and proportional to the length of charged tracks crossing the water.

The electronics for the detectors are housed in a box outside the tanks and communicate with a base station through a radio WLAN, operating in the 915 MHz band. The stations are powered by a bank of two special 12 V batteries, which are fed by two solar panels of 55 W each. The time synchronization of the tanks is based on a GPS system, capable of a time alignment precision of about 10 ns (Pryke et al [1995]). A 7 GHz microwave backbone links the base stations to the central data acquisition station (CDAS), at the campus of Malargüe in the southern site (Figure 1).

Each detector station has a two level trigger, a hardware implemented T1 and a software T2. The T1 trigger is decided in a PLD (Programmable Logical Device) (Suomijarvi et al. [2004], Szadkowski and Nitz [2004]), set with a threshold, defined in terms of a vertical equivalent muon (VEM) crossing a tank, with a typical value of 1.75 VEM on a single 25 ns time bin, in coincidence at all working PMT's. T1 is adjusted so that its rate is about 100 Hz. T2 limits the trigger rate at each station to less than 20 Hz, so as not to saturate the radio bandwidth available. The event trigger (T3) is set at CDAS combining the triggers of contiguous individual stations. The requirement in the number of stations triggered, sets the lower energy threshold. Typically, four stations are required for a threshold of 10^{19} eV. The communication between the central campus and the individual stations is bi-directional to allow the T3 trigger request the data to be downloaded to the CDAS system. Figure 5 shows a schematic view of the components of a surface detector station.

The calibration of the surface stations is done continuously. At every minute the histogram of low energy particles is taken, correspondinding roughly to about 100 000 events, mostly atmospheric muons coming from all angles into the detector. Figure 6 shows a the histogram for a surface station, taken at a prototype detector.

The incoming angle of a shower is reconstructed from the timing of arrival of the signals in the tanks. The detectors have a large cross section even for a shower with very high zenith angle, so that Auger is quite sensitive

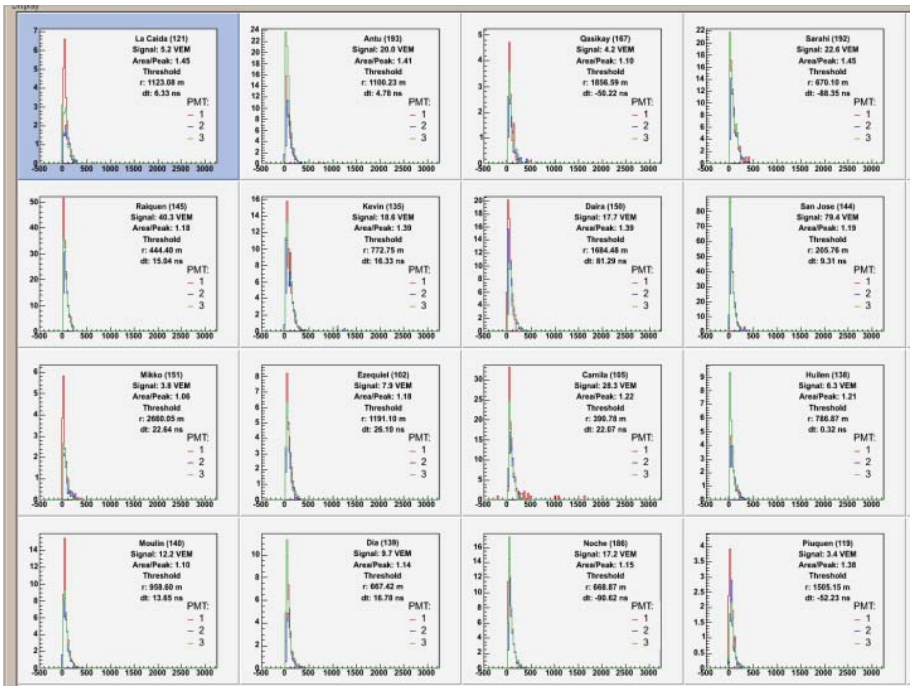

Figure 7: A typical old shower with a zenith angle of 81°. The lateral distribution function is flatter, with the signals decreasing slowly with distance to the core. The FADC traces are sharp, less than 100 ns at all core distances. No EM content, even close to the core, only muons at all distances.

to neutrinos (Bertou et al. [2002], Capelle et al. [1998]). A highly inclined shower, originating from a hadronic cosmic ray, has a very characteristic signature, having lost a substantial part of its electromagnetic component, with only a core of energetic muons remaining. The muons arrive concentrated in time, generating signals with a very sharp peak. An example of such, with the traces registred by the stations for a shower with a zenith angle of 81°, is shown in Figure 7. In contrast, a shower which has a large electromagnetic component is spread in time, with a much more complex structure, as can be seen in Figure 8, showing the traces of a shower with a 40° angle.

3.2. THE FLUORESCENCE DETECTOR

The Fluorescence Detector (FD) is composed of 4 eyes disposed on the vertices of a diamond-like configuration, with a separation of 65.7 km along the axis South-North (actually this axis is tilted by 19° into Northeast) and 57.0 km in the West-East direction (tilted by 20° into Southeast). They are at the periphery of the ground array and all stations of the SD are contained in the field of view (FOV) of the FD telescopes.

Each eye has six independent telescopes, each with a field of view of 30° in azimuth and 28.6° in elevation, adding to a 180° view of the array. Figure 9 shows the building of the Coihueco eye located on the west side of the array (see Figure2). The fluorescence light is collected by a mirror with a radius of 3.4 m and reflected into a camera, located at the focal surface of the mirror. The telescopes use a Schmidt optics design to avoid coma aberration, with a diaphragm, at the center of curvature of the mirror, with an external radius of 0.85 m. The advantage of this scheme is to project a point of light in the sky into a reasonably homogeneous spot, at the focal surface, of 0.25° radius.

The shape of the telescope mirror is a square with rounded corners with a side of 3.8 m. The radius of the diaphragm may be enlarged to 1.1 m, by adding a corrector lens annulus on the area with radius between

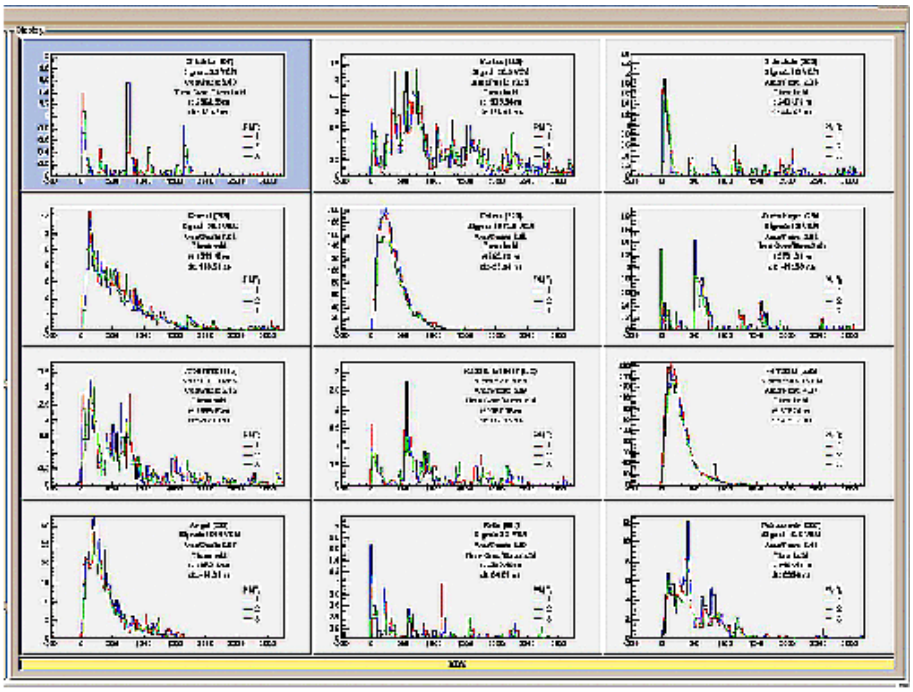

Figure 8: A typical young shower with a zenith angle of 40°. The lateral distribution function decreases quickly with the distance to the core and the FADC traces are wide, spread over several micro-seconds. There is a high EM content close to the core and spread individual muons far away.

Figure 9: The Coihueco telescope building.

0.85 m and 1.1 m (Born and Wolf [1999]) (see Figure 10). The telescope is protected from the environment by an external shutter, remotely operated (see Figure 9) and a MUG-6 UV transmitting filter, which reduces the light background.

The camera is composed by 440 pixels, each a hexagonal photomultiplier (Photonis XP3062), which monitors a solid angle of $(1.5°)^2$ projected onto the sky. The dead spaces between the photomultipliers is corrected by a reflective wedge device, called the *Mercedes corrector*, making the sky exposure very uniform.

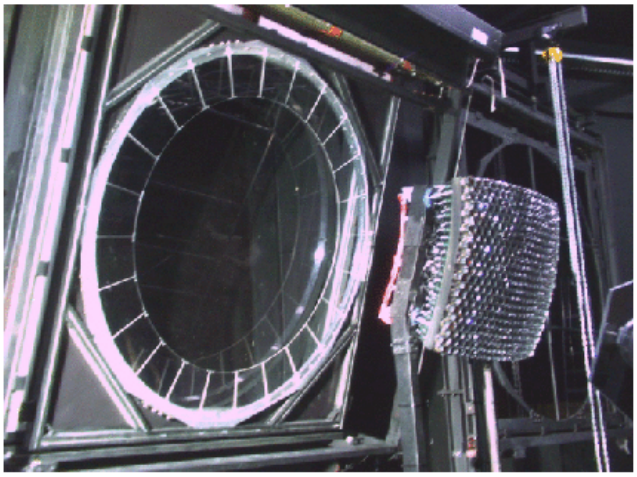

Figure 10: The diaphragm of a telescope, with corrector rings. The picture shows the camera, with its 440 pixels facing the mirror.

The electronics of the FD detector was designed to be operated remotely and with flexibility to reprogram the trigger to accommodate non-standard physical processes which may show up. The trigger rate is not limited by the transmission band available. The FD communicates with the CDAS system through the 7 GHz microwave backbone, with a capacity of 34 Mbps throughput.

To be able to operate in hybrid mode the absolute time alignment with the Čerenkov water detector must be better than 120 ns. The trigger for each FD pixel is programmed to have a rate below 100 Hz, while a special processor, with a built-in pattern recognition algorithm, keeps the overall trigger rate below 0.1 Hz. The pixels are sampled and the signal digitized at every 100 ns. The first level trigger uses a boxcar type addition of the signal over a 1 μs bin and a pixel trigger set whenever this sum is 3 σ above the background noise. An event is triggered whenever a set of 5 contiguous pixels are triggered with a time sequence associated (Kleifges et al. [2004]).

The calibration of the camera is performed by exposing the PMTs to signals from calibrated light sources diffused from an aparatus mounted on the external window of the telescopes. The camera is illuminated uniformly and the gain of each PMT characterized (Roberts et al. [2003]).

The determination of the shower energy requires an accurate estimate of the atmosphere attenuation, due to the Rayleigh (molecular) and Mie (aerosol) scattering, of the light emitted. This is done by the Horizontal Attenuation Monitor (HAM), the Aerosol Phase Function monitors (APF) and Lidar systems (Mussa et al. [2004]) mounted at each eye. The system is complemented by sky monitoring CCD's, which measures the light output of selected stars. A set of infrared cameras at each eye monitors the cloud coverage at the site. Monitoring the background noise due to stars in the field of view of the pixels are tools used to get the proper alignment of the telescopes.

The Central Laser Facility (CLF) is a steerable automatic system which produces regular pulses of linearly polarized UV light at 355nm. It is located in the middle of the array, 26 km away from Los Leones and 34 km from the Coiheco eye. This system provides a complementary measurement of the aerosol vertical optical depth *versus* height, and the horizontal uniformity of the atmosphere across the aperture of the array. This system creates artificial cosmic rays by feeding a signal into a nearby tank, monitoring the relative timing between the FD and the SD detectors.

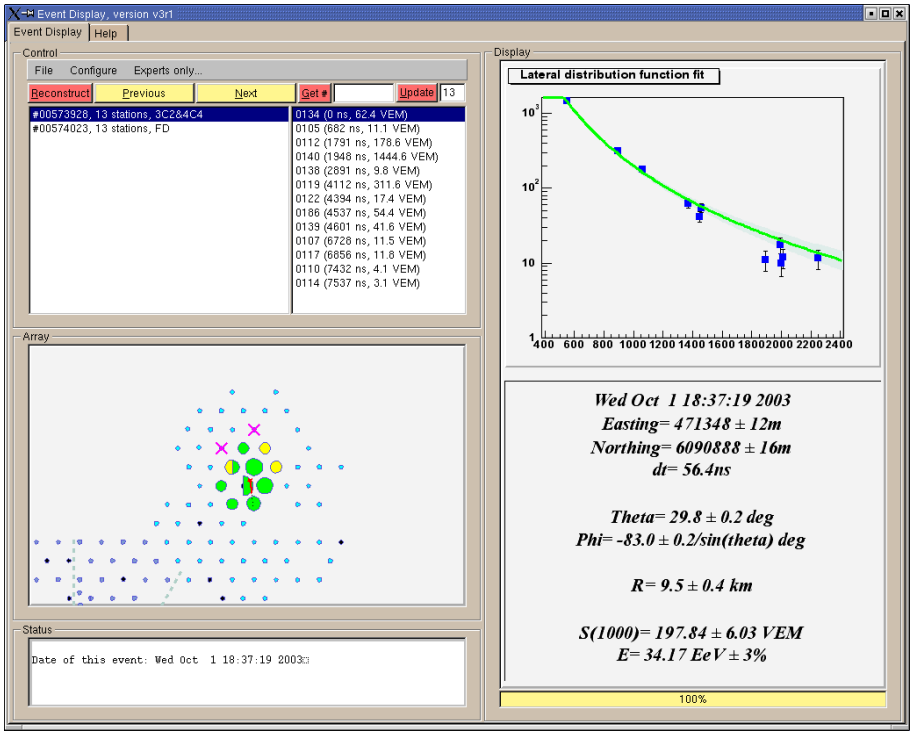

Figure 11: A typical event registred by the SD system. The shower has a zenith angle of 30° and 10 stations are used in the fitting of the lateral distribution function. The signal is quoted in VEM (Vertical Equivalent Muon).

3.3. Auger data

Since the begining of operations, in 2001, Auger has been taking data continuously, first in the Engineering Array mode, already reported (Abraham et al [2004]). At the time of this writing (November 2004) there are already more than 500 tanks fully operational and two complete eyes (Los Leones and Coihueco), half of the FD system, are running. A typical example of an event recorded by the SD system is shown in the Figure 11. The energy of the shower is infered from the lateral distribution function (LDF), fitted from density of particles hitting each tank at distinct distances (Dai et al. [1988], Hillas [1971]). The density of particles at 1 km from the core, S(1000) is quite independent of the nature of the primary cosmic ray, according to distributions extracted from shower simulation programs. Each station in the array is continuously calibrated by collecting at regular intervals signals generated by single muons. From this signal the value of a VEM (vertical equivalent muon) is extracted, taking into account variations in the atmospheric temperature and pressure.

The Auger ground stations are sensitive to very inclined showers once it has a reasonable cross-section due to the 1.2 m column of water. The very inclined showers will have transversed a larger amount of atmospheric matter before hitting the station and a large part of the electromagnetic shower will have disapeared, allowing for a much larger relative muon component. An example of this class of event is displyed in Figure 12 with a shower hitting 31 stations, coming with a zenith inclination of 86°. We show in the Figure 13 an example of an event with a very large energy, hitting 38 stations. A preliminary estimate of the energy of this shower points to values around 10^{20} eV.

The structure of the FD events are exhibited in Figures 14 and 15, taken from the event monitoring system. On both figures the map of the pixels are shown as if one would be facing the sky. So, the first event, a typical low energy shower, is flying top-down, right to left. The histogram on the top-right of the display shows the time structure of the signal in a selection of the pixels. The colour code is there just to correlate the pixel and

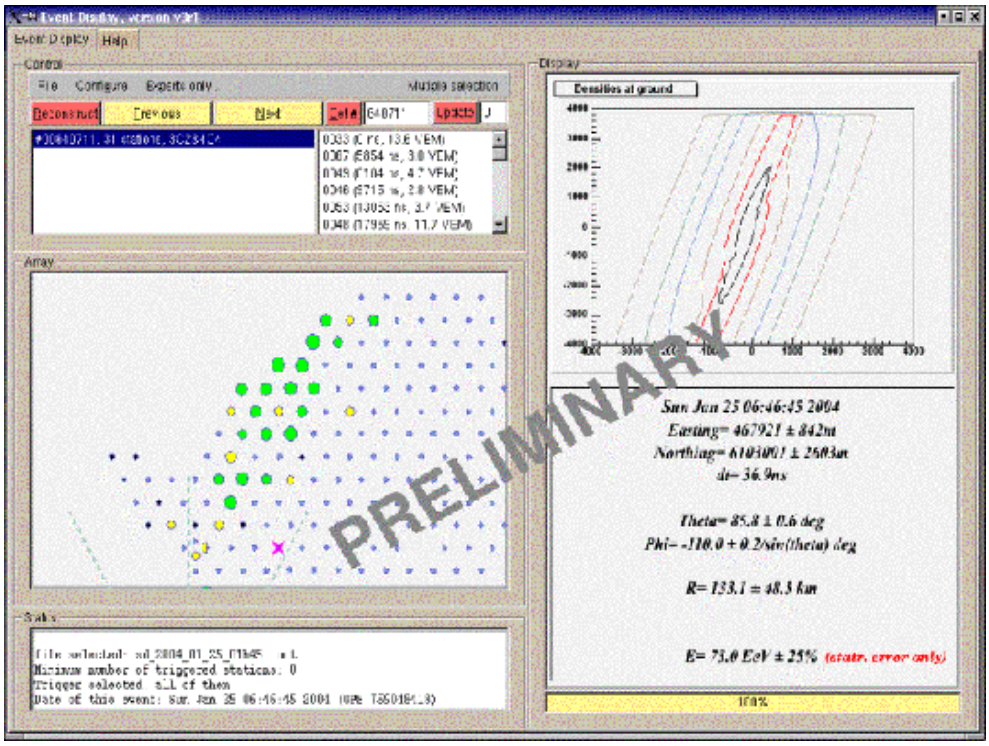

Figure 12: Event with a large zenith angle, 86° in this case. Most of the signal is carried by the surviving muons, once a large part of the electromagnetic shower has been dissipated.

the signal. Each bin on the right plot corresponds to 100 ns, so that the span of the signal from 260 to 360 units, actually corresponds to a time interval of 10μs. Figure 14 represents a typical event propagating downwards, while the Figure 15 is an laser shot event, with a time structure going upwards.

To reconstruct the geometry of the shower, first the shower detector plane (SDP) is infered by optimizing the line of light crossing the camera, using the signals as weight. The best estimate of the normal vector to the SDP, $\vec{n}_{SDP}$, is obtained by minimizing

$$\chi^2 = \sum_i w_i [\vec{n}_{SDP} \cdot \vec{r}_i]^2$$

where the signal measured in pixel i is used with the weight w_i and the $\vec{r}_i$ corresponds to the direction pointing to the source in the sky. The three dimensional geometry is recovered using the angular velocity of the signal. For each shower pixel i the average time of the arrival of the light at that pixel field of view, t_i, is determined from the FADC traces. The expression (Sommers [1995]),

$$t_i = t_0 + \frac{R_p}{c} \tan\left[\frac{(\chi_0 - \chi_i)}{2}\right],$$

allow for a fitting of the shower parameters, R_p, χ_0 and t_0. Here, c is the velocity of light, R_p the shower distance of closest approach to the detector and t_0 the time at which the shower point reaches the position of closest approach. χ_i, indicated on Figure 16, is the direction of the pixel i projected onto the SDP and χ_0 is the angle between the shower axis and the direction from the detector to the shower landing point. Figure 17 shows an example of time *versus* angle plot for a shower seen in stereo mode. However, this procedure is not free of ambiguities, which can be resolved with the input from the SD system. The timing information and location

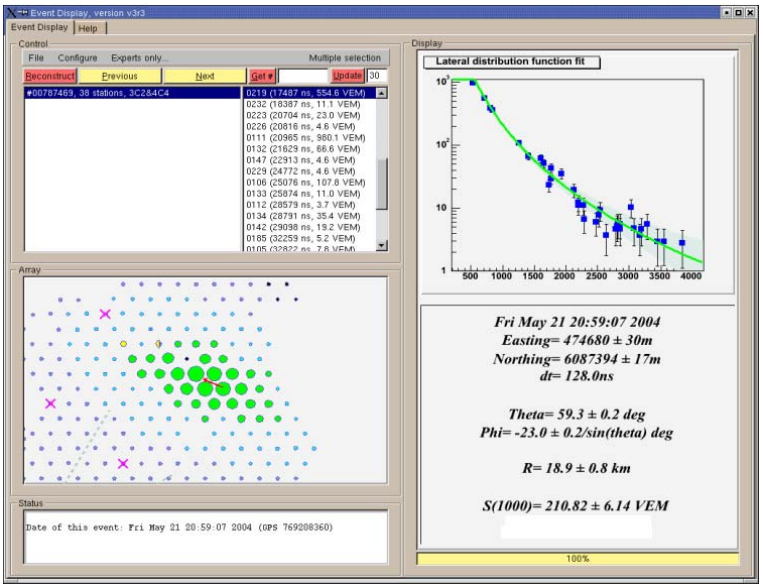

Figure 13: A large energy event, were 38 tanks triggered. The preliminary estimate for the energy, based on the lateral distribution value at 1000 m, S(1000) = 211 VEM, put it around 10^{20} eV.

from a station closest to the shower landing point can be related to the time t_0,

$$t_0 = t_{tank} - \frac{\vec{R}_{tank} \cdot \vec{S}_{hw}}{c},$$

where $\vec{R}_{tank}$ is the vector connecting the fluorescence detector to the ground station and $\vec{S}_{hw}$ is the unit vector associated to the shower propagation.

To measure the energy, the light emitted by the source is reconstructed making the corrections for the atmosphere attenuation and than subtracting the Čerenkov component of the signal, identifying the fluorescence component. The time profile and the longitudinal profile for the event exhibited above is shown in Figure 18 for both views of the event. The line fitting the longitudinal profile represents the Gaisser-Hillas function (Gaisser and Hillas [1977]).

Although there is much work to do to improve the quality of the measurements done with the SD and FD components, there are some preliminary tests that points to overall quality of the data. In particular, the correlation in the estimation of the energy of hybrid events, measured by the SD and the FD, is quite consistent.

4. SUMMARY

The Pierre Auger Observatory is a major tool to unravel the mysteries of the ultra high energy cosmic rays. The conceptual design was succesfully tested in the Engineering Array, and the partial results so far, allow us to be optimistic that the full Observatory will succeed in carrying the program to measure the energy, direction and chemical composition of these cosmic particles. In its final form, adding the Northern site, the Observatory will expose 6 000 km^2 of detectors in the ground array, coupled with a system of overlooking fluorescence detectors, with 4π sky coverage. The high statistics sample collected and the accuracy in the determination of direction of arrival, will allow for a clear picture of the nature and origin of these cosmic rays.

The hybrid mode operation offers a way to cross-calibrate the detectors and improves the energy and angular resolution of the observatory. For showers with energies above 10^{19} eV (10 EeV), the triggering efficiency is above 90%, while it reaches virtually 100% at 100 EeV. The energy resolution for showers of 10 EeV is estimated

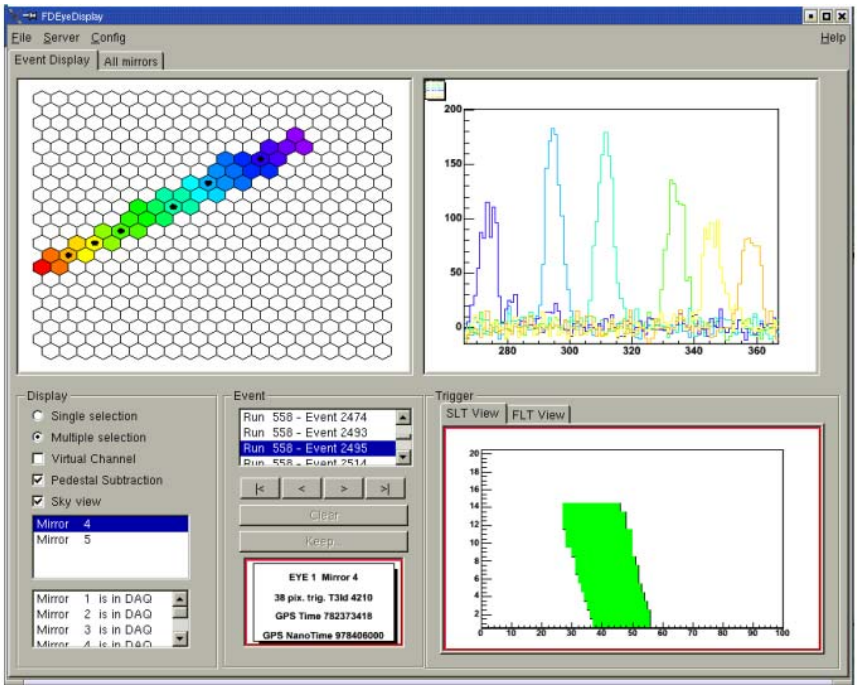

Figure 14: Typical low energy FD event. The camera display represent the shower projected on the sky. The color code just identify the pixel. The black dots on the pixels mark those exhibited on the right. The time axis on the right side histogram is set in units of 100 ns, the label 350 means 35 μs.

to be around 30% for the SD operating alone, improving to better than 20% for the hybrid mode of operation. At 100 EeV the resolution is improved quite a lot, to 15% and 10% respectively. As for the angular resolution at 100 EeV, it is estimated to be 1° for operation with the surface detector alone, but goes down to 0.20° in the hybrid mode. The statistics for the 100 EeV cosmic rays is expected to increase ten-fold in relation to the number of showers measured up to date in just one year of full operation of the Observatory.

Acknowledgments

Work supported by the Conselho Nacional de Desenvolvimento Científico e Tecnológico (CNPq), Brazil.

References

F. A. Aharonian et al, Nature **432**, 75 (2004).

Auger Collaboration, *The Pierre Auger Observatory Design Report*, FERMILAB-PUB-96-024 (1996).

Auger Collaboration, *The Pierre Auger Observatory Technical Design Report*, (http://www.auger.org/admin) (2001).

Auger Collaboration, J. Abraham et al., Nucl. Instr. Meth. **A 523**, 50 (2004).

X. Bertou, P. Billoir, O. Deligny, C. Lachaud, and A. Letessier-Selvon, Astropart. Phys. **17**, 183 (2002).

D. J. Bird et al., Phys. Rev. Lett. **71**, 3401 (1993).

C. B. Bonifazi, Ph.D. thesis, Departamento de Física, Universidad de Buenos Aires (2004).

M. Born and E. Wolf, *Principles of Optics*, vol. 1 (Cambridge Univ. Press, Cambridge, 1999), 7th ed.

K. S. Capelle, J. W. Cronin, G. Parente, and E. Zas, Astropart. Phys. **8**, 321 (1998).

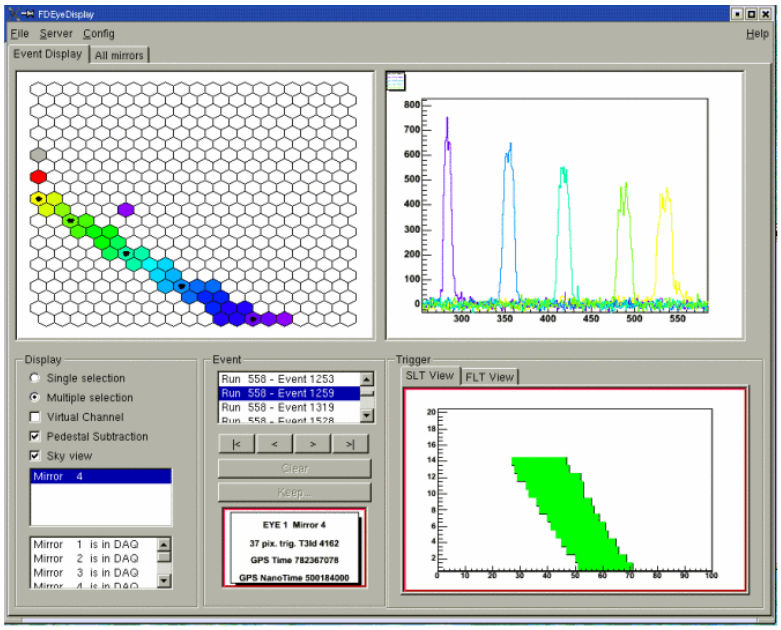

Figure 15: Laser shot event, where the light goes from the ground up.

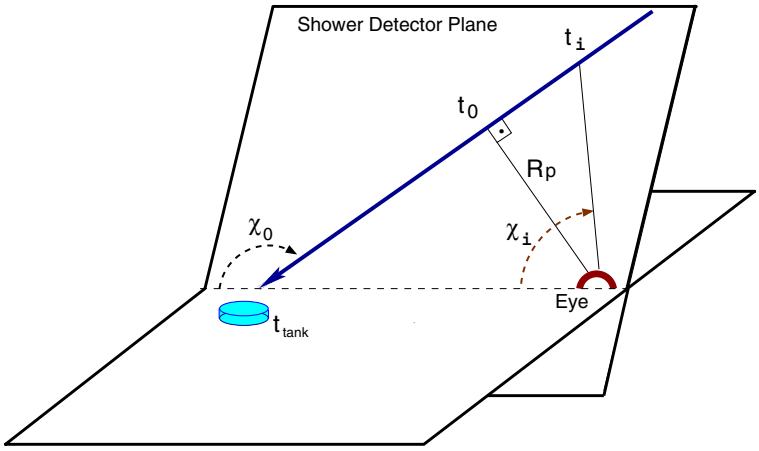

Figure 16: Shower detector plane.

J. W. Cronin, Rev. Mod. Phys. **71**, S165 (1999).

H. Y. Dai, K. Kasahara, Y. Matsubara, M. Nagano, and M. Teshima, J. Phys. G **14**, 793 (1988).

N. N. Efimov et al., *Proc. Intl. Symp. on Astrophysical Aspects of the Most Energetic Cosmics Rays* (eds. M. Nagano and F. Takahara, World Scientific, Singapore, 1991), p. 20.

T. K. Gaisser and A. Hillas, *Proccedings of the 15th International Cosmic Ray Conference* (Plovdiv, 1977), vol. 8, p. 353.

K. Greisen, Phys. Rev. Lett. **16**, 748 (1966).

A. M. Hillas, Acta Phys. Acad. Sci. Hung. **29**, 355 (1970).

A. M. Hillas, in *Proc. of the 12th ICRC* (1971), vol. 3, p. 1001.

M. Kleifges et al. (Auger Collaboration), Nucl. Instr. Meth. A **518**, 180 (2004).

M. A. Lawrence, R. J. O. Reid, and A. A. Watson, J. Phys. G **17**, 733 (1991).

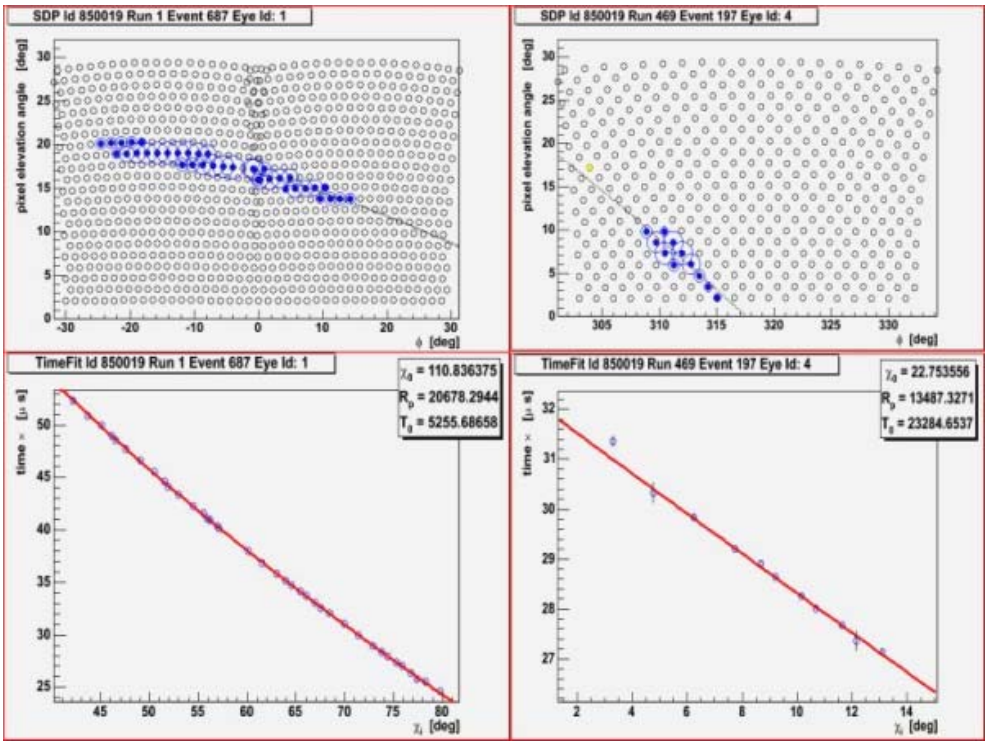

Figure 17: Event seen in stereo mode. The left hand side is the view from Los Leones and the right from Coihueco. The lower plots shows the time *versus* angle correlation as seen by each eye. The fit parameters are shown in the plots.

J. Linsley, Phys. Rev. Lett. **10**, 146 (1963a).

J. Linsley, *Proc. 8th International Cosmic Ray Conference* (1963b), vol. 4, p. 295.

M. S. Longair, *High Energy Astrophysics, Vol1: Particles, photons and their detection*, vol. 1 (Cambridge Univ. Press, Cambridge, 1992), 2nd ed.

R. Mussa, S. Argiro, R. Cester, M. Chiossa, A. Filipic, M. Horvat et al., Nucl. Instr. Meth. **A 518**, 183 (2004).

M. Nagano and A. A. Watson, Rev. Mod. Phys. **72**, 689 (2000).

M. Nagano, K. Kobayakawa, N. Sakaki and K. Ando, Astropart. Phys. **22**, 235 (2004).

A. V. Olinto, Phys. Rep. **333-334**, 329 (2000).

C. Pryke et al., Nucl. Inst. Methods **A354**, 354 (1995).

M. D. Roberts et al. (Auger Collaboration), in *Proc. 28th ICRC (Tsukuba)*, edited by T. K. et al. (2003), vol. 1, p. 453.

M. A. Shea and D. F. Smart, *19th international cosmic ray conference* (La Jolla, USA, 1985), vol. 4, p. 501.

P. Sommers, Astropart. Phys. **3**, 349 (1995).

T. Suomijarvi et al. (Auger Collaboration), Nucl. Phys. B (Proc. Suppl. **136**, 393 (2004).

Z. Szadkowski and D. Nitz, subm. Nucl. Instr. Meth. (2004).

M. Takeda et al., Phys. Rev. Lett. **81**, 1163 (1998).

R. Walker and A. A. Watson, J. Phys. G **7**, 1297 (1981).

R. Walker and A. A. Watson, J. Phys. G **8**, 1131 (1982).

S.Yoshida, H. Dai, C. C. H. Jui and P. Sommers, Astrophys. J. **479**, 547 (1997).

G. T. Zatsepin and V. A. Kuzmin, Sov. Phys. JETP Lett. **4**, 78 (1966).

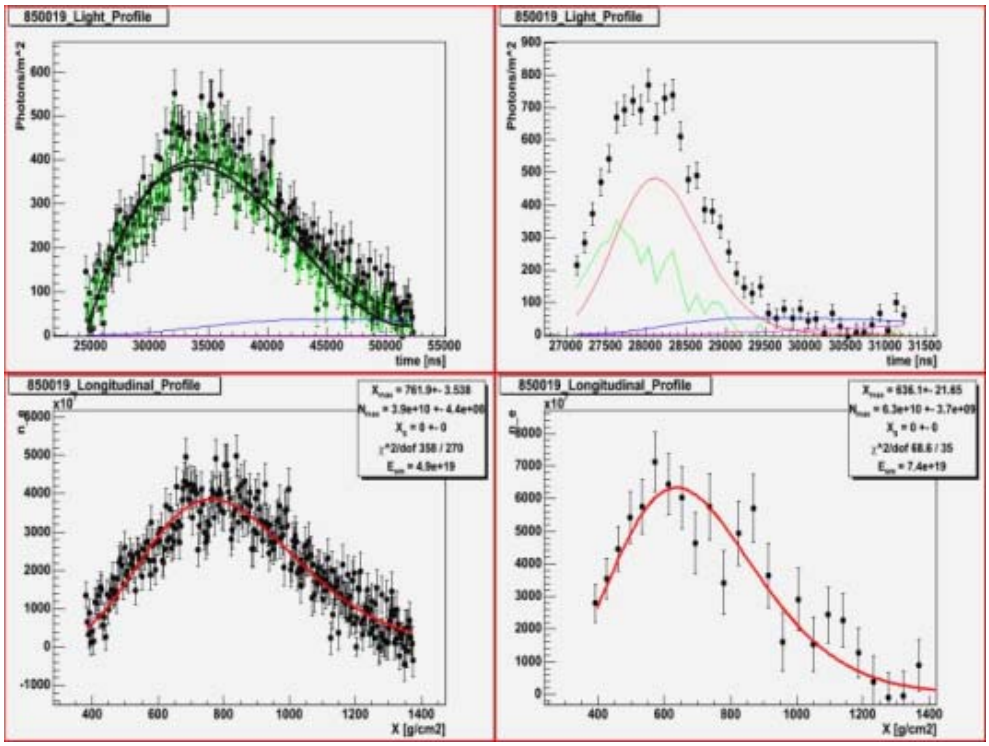

Figure 18: The time profile and the longitudinal profile of the event shown in figure 17.